ACS APPLIED MATERIALS & INTERFACES

Research Article

www.acsami.org

Controlling Surface Termination and Facet Orientation in Cu_2O Nanoparticles for High Photocatalytic Activity: A Combined Experimental and Density Functional Theory Study

Yang Su,[†,⊥] Hongfei Li,[†,⊥] Hanbin Ma,[†] John Robertson,[†] and Arokia Nathan*[,†]

[†]Department of Engineering, University of Cambridge, Cambridge CB3 0FA, U.K.

Supporting Information

ABSTRACT: Cu_2O nanoparticles with controllable facets are of great significance for photocatalysis. In this work, the surface termination and facet orientation of Cu_2O nanoparticles are accurately tuned by adjusting the amount of hydroxylamine hydrochloride and surfactant. It is found that Cu_2O nanoparticles with Cu-terminated (110) or (111) surfaces show high photocatalytic activity, while other exposed facets show poor reactivity. Density functional theory simulations confirm that sodium dodecyl sulfate surfactant can lower the surface free energy of Cu-terminated surfaces, increase the density of exposed Cu atoms at the surfaces and thus benefit the photocatalytic activity. It also shows that the poor reactivity of the Cu-terminated Cu_2O (100) surface is due to the high energy barrier of holes at the surface region.

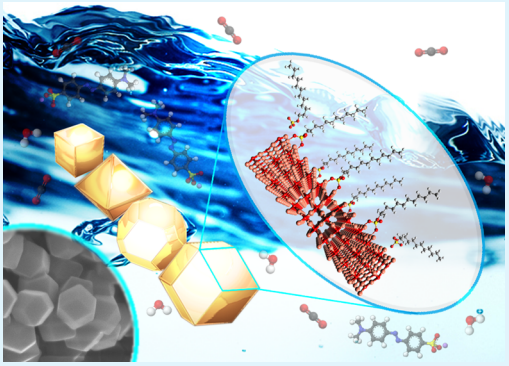

KEYWORDS: *photocatalyst, cuprous oxide, DFT, surface termination, facet orientation*

1. INTRODUCTION

Semiconductor photocatalysts have raised significant research interests due to their promising applications in both solar energy conversion and environmental purification.[1−5] Cuprous oxide (Cu_2O) is a p-type semiconductor with a direct band gap of 2.0−2.2 eV that has shown great potential for photocatalysis.[6] Cu_2O can be synthesized by low-cost means, including hydrothermal methods[7] or electrodeposition.[8] Cu_2O photocatalysts demonstrate the advantages of high efficiency, low toxicity, and environmental acceptability.[9] On the other hand, Cu_2O is also able to effectively take the advantage of visible light compared to conventional materials such as TiO_2, which needs to be activated by UV light due to its wide band gap.

Cu_2O nanoparticles could come in different architectures, e.g. cube,[10] octahedral,[11] rhombic dodecahedral,[12] truncated octahedral,[13] and 18-facet polyhedral.[14] The basic low-index facets are (100), (111), and (110), and their facet-dependent properties such as conductivity,[15] stability,[16] and photocatalytic activity[17] have been carefully studied. Cu_2O (100) facets are known to show low photocatalytic activity, while (111) and (110) facets are reported to have higher reactivity. Various surface atomic arrangements have been proposed to explain the facet-dependent properties.[18−20] Sodium dodecyl sulfate (SDS) surfactant is frequently engaged in the preparation of Cu_2O nanocrystals to tailor the growth and morphology of Cu_2O. SDS is reported to show preferential adsorption on different facets according to the reaction conditions.[8] However, the effects on the atomic arrangements and photocatalytic activity of various facets of SDS adsorption still remain unclear.

The density functional theory (DFT) method has been widely applied to study the physical and chemical properties of Cu_2O. Soon et al. reported a detailed investigation of surface free energy for various surface orientations, terminations, and reconstructions.[21] Le et al. found O-terminated surfaces to be energetically more favorable than Cu-terminated surfaces for a wide range of pressures and temperatures.[22] Bendavid et al. reported the DFT results of the band edge and redox potential analysis,[23] and Kwon et al. expanded the thermodynamic stability results to higher Miller index surfaces.[16] However, the reported literature deals with only clean Cu_2O surfaces without considering the effect of surfactants, e.g. SDS, while the surfactant is actually used to modify the morphology of Cu_2O surfaces. Therefore, the thermodynamic stability of various Cu_2O surfaces with the impact of surfactants is actually unclear. Moreover, these DFT results on Cu_2O apply mostly to the simple generalized gradient approximation (GGA) exchange correlation functional to calculate structural and electronic properties.[16,21] This GGA functional is well-known to severely underestimate the bandgap of semiconductor and give orbitals that are too delocalized. Specifically, the GGA can predict only a band gap of less than 1 eV for Cu_2O rather than the experimental value of 2.0−2.2 eV. In addition, the Cu_2O surfaces involve quite a high density of dangling bonds, and these orbitals are poorly described by GGA. Thus, it is unclear whether the Cu_2O surface thermodynamic stability predicted

Received: December 6, 2016
Accepted: February 16, 2017
Published: February 16, 2017

DOI: 10.1021/acsami.6b15648
ACS Appl. Mater. Interfaces 2017, 9, 8100−8106

by GGA is reliable. Hybrid functionals, e.g. the Heyd, Scuseria, Erzernhof (HSE) functional[24] or screened exchange (sX) functional,[25] are known to fix these errors well and are also computationally acceptable for supercells of 100−200 atoms needed for the surface model calculation. Thus, it is preferable to use these hybrid functionals rather than the GGA functional to calculate the thermodynamic stability of Cu_2O clean surfaces and surfactant-applied surfaces.

In this work, we synthesized Cu_2O nanocrystals with various morphologies using a facile hydrothermal method. The architectures and exposed facets of Cu_2O nanoparticles were precisely controlled by adjusting the amount of hydroxylamine hydrochloride and SDS. The morphology evolution was observed with the increase in added SDS. Facets with the same orientation are demonstrated to show different photocatalytic activity when different amounts of SDS are introduced, indicating that SDS tailors the atomic structure and thus the reactivity of Cu_2O facets. The mechanism was studied using DFT simulations with the sX functional. Facets with a high density of surface copper dangling bonds become energetically more favorable in the presence of SDS, leading to higher reactivity. The photocatalytic activity of the Cu-terminated Cu_2O (100) surface is limited by the large energy barrier for holes at the surface, which suppresses the transferring of holes from the bulk region to the surface region.

2. METHODOLOGY

2.1. Materials. All chemicals were used as received without further purification. The copper(II) chloride (97%), hydroxylamine hydrochloride (99%), SDS (98.5%), sodium sulfate (99%), and methyl orange (100%) were purchased from Sigma-Aldrich, and sodium hydroxide (98%) was purchased from Fisher.

2.2. Synthesis of Cu_2O Nanocrystals. Cu_2O nanocrystals were synthesized using the hydrothermal method. This was reported in our previous work.[26] Sixty-seven milligrams of $CuCl_2$ and different amounts of SDS were dispersed in 65 mL of deionized water. The solution was placed in a water bath set at 35 °C with vigorous stirring for 10 min. Ten milliliters of 0.2 M NaOH was introduced. Twenty-five milliliters of $NH_2OH{\cdot}HCl$ with various concentrations was added to the precursors. The solution was stirred for 30 s and kept in the water bath for 1.5 h. The products were centrifuged at 5000 rpm for 4 min, and the precipitate was washed and centrifuged twice using 50 mL of water and ethanol. The obtained product was then dried in the oven at 60 °C for 12 h. The products were labeled as A-B, in which A is the weight of SDS added in grams and B is the concentration of $NH_2OH{\cdot}HCl$ added in moles. For instance, sample (0.5-0.4) denotes that 0.5 g of SDS and 25 mL of 0.4 M $NH_2OH{\cdot}HCl$ were used in sample preparation.

2.3. Nanocrystal Characterization. The morphology of synthesized nanocrystals was characterized using Leo Gemini 1530VP scanning electron microscopy (SEM) at 8 kV. X-ray diffraction (XRD) patterns were obtained by a Bruker D8 Advance diffractometer with Cu Kα radiation. X-ray photoelectron spectroscopy (XPS) measurements were performed using a PHI5000VersaProbe II scanning XPS microscope. The Brunauer−Emmett−Teller (BET) surface area was measured by Micromeritics Gemini VII.

2.4. Photocatalysis Experiment. White light LEDs were used as the light source. The spectra of the light source were measured using a Labsphere CDS-600 spectrometer. The photocatalysis experiment on the degradation of MO was carried out in a homemade quartz immersion reactor with a volume of 330 mL at room temperature. One portion of pristine Cu_2O photocatalysts was dispersed in 300 mL of 20 mg/L MO solution. The solution was constantly stirred in the dark for 15 min to reach an adsorption and desorption equilibrium. Every 30 min, 1.5 mL of the solution was sampled and centrifuged at 5000 rpm for 4 min to separate the photocatalysts from the solution. The UV−vis absorption spectra of the samples were recorded, and the concentration of MO was determined by the absorption at 464 nm using UniCam UV−vis spectrometer v.2.

2.5. DFT Simulation. The DFT simulations were carried out using the CASTEP plane wave pseudopotential code.[27] The norm-conserving pseudopotential was used with a cutoff energy of 750 eV in all calculations. The Cu_2O surface structures were calculated by the GGA exchange correlational functional with the 3 × 3 × 1 Monkhorst−Pack K-points scheme. The geometry optimization was carried out until the residual force on each atom was smaller than 0.01 eV/ Å. The screened exchange (sX) hybrid functional was applied in all electronic property calculations to correct the well-known band gap error to yield the correct electronic properties.

Six slab models were built to investigate Cu_2O (100), (110), and (111) facets-terminated by O or Cu atoms. In each model, the slab was over 15 Å thick, and a 15 Å vacuum was inserted to suppress the interaction between the slab and its image due to the periodic boundary condition.

The surface energy of the Cu_2O surface in this paper is defined as

$$\gamma = \frac{1}{2A}\left(E_{\text{Slab}}^{\text{tot}} - \frac{1}{2}[N_{\text{Cu}}E_{\text{bulk}}^{\text{tot}} + (2N_{\text{O}} - N_{\text{Cu}})\mu_{\text{O}}]\right) \quad (1)$$

where $E_{\text{Slab}}^{\text{tot}}$ is the total energy of the slab model, $E_{\text{bulk}}^{\text{tot}}$ is the total energy of bulk Cu_2O crystal per formula unit, N_{Cu} and N_{O} are the number of Cu and O atoms in the model, respectively, A is the surface area of the slab, and μ_{O} is the oxygen chemical potential, which is determined by the environmental condition.

The lower boundary of O chemical potential (O-poor limit) is taken as the equilibrium between Cu_2O and Cu metal, while the upper boundary (O-rich limit) is usually assumed to be the equilibrium between Cu_2O and the oxygen molecule.[21] However, we propose that in an O-rich condition, Cu_2O can be slowly oxidized to CuO. Therefore, the O-rich limit should be taken as the equilibrium between Cu_2O and CuO. Herein, the relative oxygen chemical potential was defined, and the oxygen molecule was used as the zero reference:

$$\Delta\mu_{\text{O}} = \mu_{\text{O}} - \mu_{\text{O}}(\text{O}_2)$$

Thus, the range of $\Delta\mu_{\text{O}}$ could be determined by the following condition:

$$H_{\text{f}}(\text{Cu}_2\text{O}) \le \Delta\mu_{\text{O}} \le H_{\text{f}}(\text{CuO}) < 0$$

where $H_{\text{f}}(Cu_2O)$ and $H_{\text{f}}(CuO)$ are the standard heat of the formation of Cu_2O and CuO, respectively.

3. RESULTS AND DISCUSSION

3.1. Morphology of Cu_2O Nanocrystals. Cu_2O nanocrystals with various morphologies were obtained, as shown in Figure 1. The morphologies and exposed facets are highly dependent on the hydrothermal condition. Cubic (0-0.17), 26-facet (0-0.4) and truncated rhombic dodecahedral (0-1.0) structures are observed with the increase in the concentration of added $NH_2OH{\cdot}HCl$, where no SDS is present. Each cubic Cu_2O nanocrystal has 6 exposed (100) facets. The 26-facet architecture has 6 (100) facets, 8 (111) facets, and 12 (110) facets. Twelve (110) facets and 6 (100) facets are observed for the truncated rhombic dodecahedral structure. The particle size is not uniform due to the absence of surfactant. Morphology evolution is observed with the increase in added SDS, while other conditions are kept the same. The cubic structure remains unchanged when 0.5 g of SDS (0.5-0.17) and 1 g of SDS (1.0-0.17) are added. The 26-facet structure transforms to porous octahedron (0.5-0.4) when 0.5 g of SDS is introduced and changes to the octahedron (1.0-0.4) with 8 exposed (111) facets when 1 g SDS is added. The truncated rhombic dodecahedral architecture evolves to rhombic dodecahedron (1.0-1.0) with 12 exposed (110) facets when 1 g of SDS is introduced. The evolution of morphology indicates the

DOI: 10.1021/acsami.6b15648
ACS Appl. Mater. Interfaces 2017, 9, 8100−8106

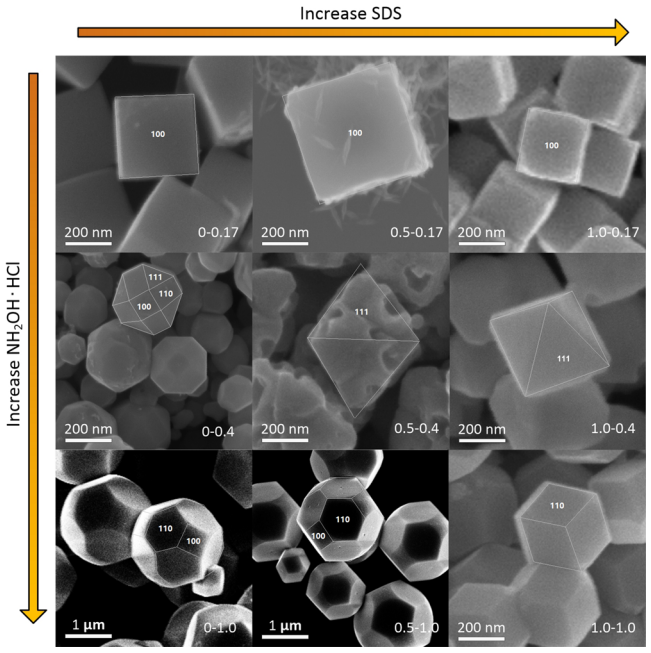

Figure 1. Morphology evolution under various hydrothermal conditions.

preferential adsorption of SDS on different facets, tailoring the growth of Cu_2O nanocrystals. The introduction of SDS also increases the uniformity of particle size. The low-magnification SEM images are shown in Figure S1. The phase and purity of the products were determined by XRD and XPS measurements. As shown in Figure S2 in the Supporting Information, the XRD pattern of the synthesized Cu_2O nanocrystals matches the standard Cu_2O XRD pattern (JCPDS No. 05-0667). The XPS peaks of Cu $2p_{1/2}$(952.28 eV) and Cu $2p_{3/2}$ (932.38 eV) imply the +1 chemical valence of Cu in the product.[28]

3.2. Photocatalytic Performance of Cu_2O Nanocrystals. The photocatalytic activity of Cu_2O nanocrystals with various morphologies and exposed facets was characterized using MO. The degradation rate of MO using Cu_2O photocatalysts under the illumination of visible LED light source within 2 h is demonstrated in Figure 2. The spectrum of the LED light source measured by a spectrometer peaks at 455 nm with no UV component (<400 nm), as shown in Figure S3 in the Supporting Information, and the measured power is 8.88 W. Samples (0-0.17), (0.5-0.17), and (1.0-0.17) with cubic structure show low efficiency in the degradation of MO, as shown in Figure 2a. Samples (0-0.4), (0.5-0.4), and (1.0-0.4) appear to have higher photocatalytic activity as the amount of added SDS is increased, as shown in Figure 2b. Low degradation efficiency is observed for samples (0-1.0) and (0.5-1.0) with larger particle size until the amount of SDS reaches 1.0 g, as demonstrated in Figure 2c. The percentage of MO removed by all 9 samples is presented in Figure 2d, where sample (1.0-1.0) shows the highest efficiency and removes nearly 98% of MO within 2 h of degradation. The stability of sample (1.0-1.0) is demonstrated in the Supporting Information, Figure S4. Over 93% of MO is degraded in the fifth cycle, indicating its high stability under visible LEDs. The low efficiency for all the samples with cubic structure indicates the poor photocatalytic activity of (100) facets, while sample (1.0-0.4) with all (111) facets and sample (1.0-1.0) with all (110) facets appear to show much higher photocatalytic activity. However, the (0-0.4) with the majority of (111) and (110) facets and particle size comparable to those of (1.0-0.4) and (1.0-1.0) appears to show much lower photocatalytic activity, indicating that even the same facets may show different activity under different hydrothermal conditions. The various photocatalytic performance implies that the introduction of SDS

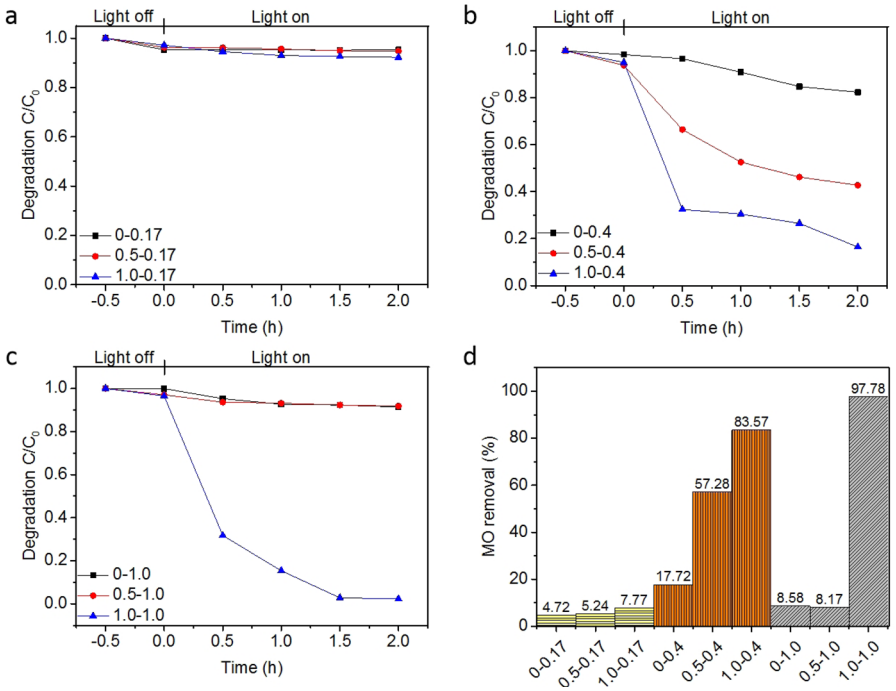

Figure 2. Degradation of MO using (a) samples (0-0.17), (0.5-0.17), and (1.0-0.17); (b) samples (0-0.4), (0.5-0.4), and (1.0-0.4); and (c) samples (0-1.0), (0.5-1.0), and (1.0-1.0). (d) MO removal by different Cu_2O photocatalysts.

DOI: 10.1021/acsami.6b15648
ACS Appl. Mater. Interfaces 2017, 9, 8100−8106

modifies the surface atomic arrangement and improves the photocatalytic activity of Cu_2O (111) and (110) facets. No dramatic enhancement of photocatalytic activity is observed for (100) facets with the increase in SDS.

3.3. DFT Simulation. The atomic structures of the Cu_2O (100), (110), and (111) surfaces are shown in Figure 3. For the

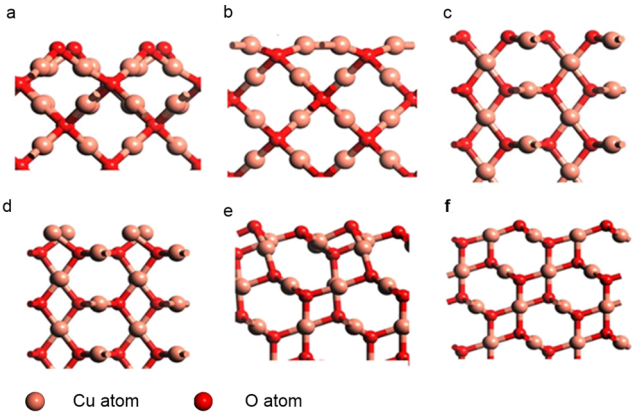

Figure 3. Atomic models of Cu_2O surfaces. (a) Cu_2O (100):O, (b) Cu_2O (100):Cu, (c) Cu_2O (110):O, (d) Cu_2O (110):Cu, (e) Cu_2O (111):O, and (f) Cu_2O (111) surfaces.

Cu_2O (100) and (110) surfaces, two termination situations, including the Cu_2O:O and Cu_2O:Cu surfaces with the stoichiometric ratio $R_{Cu/O}$ smaller and larger than 2, respectively, are considered. For the Cu_2O (111) surface, the stoichiometric of Cu_2O (111) instead of the Cu_2O (111):Cu surface is considered because the stoichiometric surface already has the exposed Cu dangling bonds at the surface and is energetically much more stable.

The heat of formation of Cu_2O and CuO bulk crystals were calculated to determine the possible range of oxygen chemical potential. It turns out that the $H_f(Cu_2O) = -1.70$ eV and $H_f(CuO) = -1.53$ eV according to simulation, which agree well with the experimental values of −1.77 and −1.62 eV, respectively.[29] These two values determine the O-rich and O-poor limits, as introduced in the Methods section.

The surface energy of these six Cu_2O surfaces as a function of oxygen chemical potential was calculated to investigate the relative thermal stability among them. The surface energy values of O-rich and O-poor limits are summarized in Table 1. It is shown that the O-terminated surfaces are energetically more favorable than Cu-terminated surfaces regardless of the value of O chemical potential for all surface directions. This conclusion is consistent with the findings by Soon et al.[21] The

Table 1. Surface Free Energy of Various Cu_2O Surfaces at O-Rich and O-Poor Conditions[a]

	clean surface		SO_4CH_3 adsorbed surface	
surface structures	γ (O-rich)	γ (O-poor)	γ (O-rich)	γ (O-poor)
Cu_2O(100):O	0.048	0.053	0.070	0.075
Cu_2O(100):Cu	0.100	0.095	0.067	0.062
Cu_2O(110):O	0.016	0.019	0.039	0.043
Cu_2O(110):Cu	0.118	0.115	0.040	0.037
Cu_2O(111):O	0.044	0.050	0.048	0.053
Cu_2O(111)	0.049	0.049	0.021	0.021

[a]Values are reported in eV/Å^2.

exact values at O-rich conditions differ from Soon's results because here, the equilibrium between Cu_2O and CuO rather than the oxygen molecule is used as the O-rich limit condition.

The partial density of states (DOS) of Cu_2O (100):Cu, Cu_2O (110):Cu, and Cu_2O (111) surfaces are shown in Figures S5a–c. The unsaturated Cu atoms at the surface give rise to some gap states which are considered to be the active sites in photocatalytic reaction. The conduction band minimum (CBM) and valence band maximum (VBM) of these surfaces are determined by analyzing the partial DOS of the bulk like middle layer atoms in the slab model, which are noted as bulk Cu and bulk O in the figures. The band edge of Cu_2O surfaces and Cu_2O bulk crystal are compared in Figure S5d, in which the bands of different models are aligned by the 3p core level of Cu at −73 eV. It is shown that the band edges of Cu-terminated Cu_2O surfaces are generally lower than those of Cu_2O bulk crystal, while the Cu_2O (110):Cu and Cu_2O (111) surfaces have a band edge lower than that of the Cu_2O (100):Cu surface. In addition, the band gap of 2.1 eV calculated by sX methods agrees well with the experimental value.

To investigate the influence of SDS on Cu_2O surface morphology, the surface energy of the SO_4CH_3 group adsorbed Cu_2O surfaces was calculated and compared with the value of clean surfaces. The atomic structures of the SO_4CH_3 group adsorbed Cu_2O surfaces are shown in the Supporting Information, Figure S6. Here, the SO_4CH_3 group is used instead of the actual adsorbing moiety of SDS, $CH_3(CH_2)_{11}SO_4$, because the long alkyl chain has little influence on the adsorption behaviors. As shown in Figure 4, Cu-terminated surfaces become energetically more favorable than O-terminated surfaces after the adsorption of SDS for all three kinds of Cu_2O surfaces within the possible range of O chemical potential. This is due to two reasons. The $CH_3(CH_2)_{11}SO_4$ group of SDS can form an O–Cu bond with the surface Cu atoms. Such chemical adsorption passivates the dangling bonds on surface Cu atoms and lowers the surface energy of Cu-terminated surfaces. Moreover, the negatively charged $[CH_3(CH_2)_{11}SO_4]^-$ group neutralizes the excess positive charge on Cu-terminated surface, thus forming the closed-shell electronic configuration and stabilizing Cu-terminated surfaces.

The in-plane averaged electrostatic potential of the Cu-terminated Cu_2O surfaces as a function of the z-coordinate was also calculated, as shown in Figure 5. The potential curve shows a number of dips at the position of each Cu and O atom because the nucleus region is positively charged. It turns out that the slab region contour of the electrostatic potential of the Cu_2O (110):Cu and Cu_2O (111) surfaces is quite flat. In other words, the surface and bulk regions have similar values of electrostatic potential for these two surfaces. However, for the Cu_2O (100):Cu surface, the electrostatic potential of surface Cu atoms lies 3.5 eV below that of middle layer Cu atoms. Such potential difference acts as a large energy barrier for positive charge carriers, which prevents mobile holes moving from the bulk region into the surface region. Therefore, the Cu_2O (100):Cu surface has a density of mobile holes much lower compared to those of the Cu_2O (110):Cu and Cu_2O (111) surfaces, which explains the poor photocatalytic activity of the Cu_2O (100):Cu surface.

3.4. Discussion. The morphologies and exposed facets of nanocrystals are accurately controlled by adjusting the hydrothermal conditions. The activity of the surface is strongly related to the value of the surface free energy. Surfaces with a

DOI: 10.1021/acsami.6b15648
ACS Appl. Mater. Interfaces 2017, 9, 8100–8106

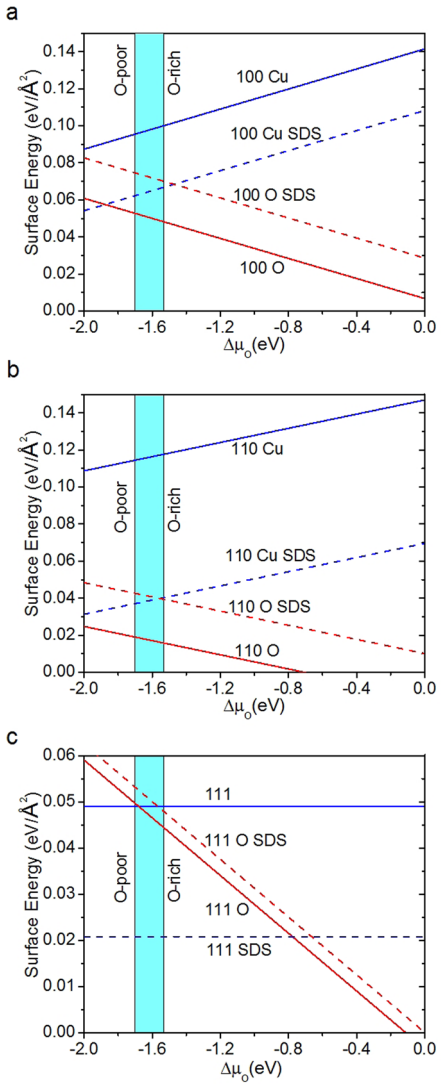

Figure 4. Calculated surface free energy of various Cu_2O surfaces: (a) (100), (b) (110), and (c) (111). The surfaces-terminated by O atoms are indicated by red lines, while those-terminated by Cu are indicated by blue lines. The solid lines indicate clean surfaces, while the dashed lines indicate Cu_2O surfaces adsorbed by the SO_4CH_3 group.

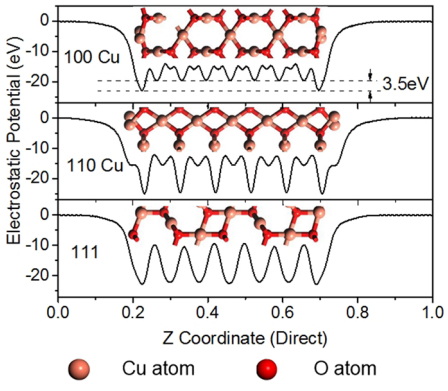

Figure 5. Averaged electrostatic potential of the Cu-terminated Cu_2O slabs as a function of *z*-direct coordinate. The vacuum level was shifted to the zero point.

low surface energy are usually stable and easy to form experimentally, but are unlikely to be reactive. On the other hand, surfaces with high surface energy are usually unstable and easy to be reconstructed in the experiment. They are prone to be reactive, which is beneficial to photocatalytic reactions. It is reported that there is a strong correlation between the photocatalytic reactivity of Cu_2O and surface Cu density. DFT simulation shows that the clean Cu-terminated surfaces generally have surface energy much higher than that of O-terminated surfaces, which is consistent with the fact that Cu_2O surfaces with exposed Cu atoms are more reactive. On the other hand, the adsorption of the SO_4CH_3 group makes Cu-terminated surfaces energetically more favorable, indicating that the SDS surfactant changes the morphology of Cu_2O facet by exposing more Cu sites at the surface.

DFT simulation results of the trend in surface energy and electrostatic potential explain the photocatalytic activity results well, as shown in Figure 2. Samples (0-0.17), (0-0.4), and (0-1.0) expose O-terminated surfaces, while samples (1.0-0.17), (1.0-0.4), and (1.0-1.0) with the highest amount of SDS expose Cu-terminated surfaces. This is because the O-terminated surfaces are energetically more favorable for clean Cu_2O surfaces, while Cu-terminated surfaces dominate when SDS is adsorbed on the surface. The Cu-terminated surfaces have much higher photocatalytic reactivity because the exposed Cu atoms with dangling bonds play an important role in photocatalytic reactions. The sample (1.0-1.0) shows the highest photocatalytic activity because the Cu_2O (110):Cu surface has a high density of surface unsaturated Cu atoms. Its high ratio of active facets also contributes to its higher reactivity compared to those of samples (0-1.0) and (0.5-1.0), which expose some inactive Cu_2O (100) facets. Sample (1.0-0.4) shows the second highest photocatalytic activity because the Cu_2O (111) surface also has surface unsaturated atoms but of a slightly lower density. In addition, the Cu_2O (110):Cu and Cu_2O (111) surfaces have a band edge lower than that of the Cu_2O (100):Cu surface, which provides photogenerated holes with higher energy. It favors the injection of holes from VBM of Cu_2O into MO and facilitates the photocatalytic reaction. To best compare the photocatalytic activity of Cu_2O (110):Cu, Cu_2O (111), and Cu_2O (100):Cu surfaces, samples (1.0-0.17), (1.0-0.4), and (1.0-1.0) with a calculated surface area of 0.1 m^2 according to their BET surface area as presented in Figure S7a were added to 300 mL of a 20 mg/L MO solution for photocatalytic degradation testing. More than 90% of MO is degraded by sample (1.0-1.0), while 40% is degraded by sample (1.0-0.4), as shown in Figure S7b. Sample (1.0-0.17) turns out to show very low photocatalytic activity. This result confirms that Cu_2O (110):Cu has the highest photocatalytic activity. The degradation toward various organic pollutants in industrial wastewater and toluene using sample (1.0-1.0) was reported in our previous work.[26] The as-prepared Cu_2O photocatalysts have the capability to degrade a wide range of organic compounds effectively.

It is generally accepted that Cu_2O (100) and even Cu_2O (100):Cu surfaces with a high density of exposed Cu atoms suffer from poor photocatalytic activity, but the reason is unclear. Here, we claim the mechanism to be the high energy barrier of holes at the Cu_2O (100):Cu surfaces, suppressing hole transfer from the bulk to the surface. Therefore, this surface has quite a low density of holes, which limits its photocatalytic activity.[30] This mechanism is confirmed by the photocatalytic measurement result of sample (1.0-0.17) with poor photocatalytic activity. A thorough understanding of the formation mechanism and photocatalytic activity of various

DOI: 10.1021/acsami.6b15648
ACS Appl. Mater. Interfaces 2017, 9, 8100−8106

Cu_2O facets through the combination of experiments and simulation provides us with the capability to precisely design Cu_2O architectures with active facets for highly efficient photocatalysis.

4. CONCLUSION

In this work, we successfully synthesized Cu_2O nanocrystals of various architectures and exposed facets using a facile hydrothermal method. SDS surfactant shows preferential adsorption on various Cu_2O facets depending on the hydrothermal growth conditions. Surface Cu atoms with dangling bonds play a central role in photocatalytic reactions. DFT simulations show that the adsorption of SDS on the surface of Cu_2O (100), (111), and (110) facets lowers the surface free energy of Cu-terminated surfaces and leads to the formation of active facets with a high density of Cu dangling bonds. Rhombic dodecahedral Cu_2O nanocrystals with all Cu_2O (110):Cu facets show the highest surface energy and photocatalytic activity for the degradation of MO. Cu_2O (100):Cu facets with a large energy barrier for holes at the surface show low photocatalytic activity due to deficiency of holes at the surface. The results presented here show that Cu_2O nanocrystals with Cu_2O (111):Cu and Cu_2O (110):Cu facets can serve as low-cost high-efficiency photocatalysts for environmental purification. It is imperative to understand the controllability of exposed facets and their corresponding reactivity, bringing about new capability in the design of high-efficiency structures for photocatalysis.

■ ASSOCIATED CONTENT

Supporting Information

The Supporting Information is available free of charge on the ACS Publications website at DOI: 10.1021/acsami.6b15648.

SEM images of Cu_2O nanocrystals, XRD and XPS patterns of Cu_2O nanocrystals, spectra of LED light source, cycling experiments of photocatalytic degradation of MO, partial DOS of Cu_2O facets, atomic structures of the SO_4CH_3 group adsorbed on Cu_2O facets (PDF)

■ AUTHOR INFORMATION

Corresponding Author

*E-mail: an299@cam.ac.uk.

ORCID

Yang Su: 0000-0001-5425-5920

Hongfei Li: 0000-0002-8456-5361

Author Contributions

⊥Y.S. and H.L. contributed equally.

Notes

The authors declare no competing financial interest.

■ ACKNOWLEDGMENTS

This work was funded by the Engineering and Physical Sciences Research Council under Project EP/M013650/1.

■ REFERENCES

(1) Liu, L.; Yang, W.; Li, Q.; Gao, S.; Shang, J. K. Synthesis of Cu2O Nanospheres Decorated with TiO2 Nanoislands, Their Enhanced Photoactivity and Stability under Visible Light Illumination, and Their Post-Illumination Catalytic Memory. *ACS Appl. Mater. Interfaces* **2014**, *6* (8), 5629−5639.

(2) Wang, J.-C.; Zhang, L.; Fang, W.-X.; Ren, J.; Li, Y.-Y.; Yao, H.-C.; Wang, J.; Li, Z. Enhanced Photoreduction CO2 Activity over Direct Z-Scheme α-Fe2O3/Cu2O Heterostructures Under Visible Light Irradiation. *ACS Appl. Mater. Interfaces* **2015**, *7* (16), 8631−8639.

(3) Li, J.; Cushing, S. K.; Bright, J.; Meng, F.; Senty, T. R.; Zheng, P.; Bristow, A. D.; Wu, N. Ag@Cu2O Core-Shell Nanoparticles as Visible-Light Plasmonic Photocatalysts. *ACS Catal.* **2013**, *3* (1), 47−51.

(4) Zhu, T.; Li Ong, W.; Zhu, L.; Wei, H. G. TiO2 Fibers Supported β-FeOOH Nanostructures as Efficient Visible Light Photocatalyst and Room Temperature Sensor. *Sci. Rep.* **2015**, *5* (April), 10601.

(5) Briskman, R. N. A Study of Electrodeposited Cuprous Oxide Photovoltaic Cells. *Sol. Energy Mater. Sol. Cells* **1992**, *27*, 361−368.

(6) Paracchino, A.; Laporte, V.; Sivula, K.; Grätzel, M.; Thimsen, E. Highly Active Oxide Photocathode for Photoelectrochemical Water Reduction. *Nat. Mater.* **2011**, *10* (6), 456−461.

(7) Huang, W. C.; Lyu, L. M.; Yang, Y. C.; Huang, M. H. Synthesis of Cu2O Nanocrystals from Cubic to Rhombic Dodecahedral Structures and Their Comparative Photocatalytic Activity. *J. Am. Chem. Soc.* **2012**, *134*, 1261−1267.

(8) Siegfried, M. J.; Choi, K. S. Electrochemical Crystallization of Cuprous Oxide with Systematic Shape Evolution. *Adv. Mater.* **2004**, *16* (19), 1743−1746.

(9) Zheng, Z.; Huang, B.; Wang, Z.; Guo, M.; Qin, X.; Zhang, X.; Wang, P.; Dai, Y. Crystal Faces of Cu2O and Their Stabilities in Photocatalytic Reactions. *J. Phys. Chem. C* **2009**, *113* (32), 14448−14453.

(10) Kuo, C. H.; Chen, C. H.; Huang, M. H. Seed-Mediated Synthesis of Monodispersed Cu2O Nanocubes with Five Different Size Ranges from 40 to 420 Nm. *Adv. Funct. Mater.* **2007**, *17*, 3773−3780.

(11) Xu, Y.; Wang, H.; Yu, Y.; Tian, L.; Zhao, W.; Zhang, B. Cu2O Nanocrystals: Surfactant-Free Room-Temperature Morphology-Modulated Synthesis and Shape-Dependent Heterogeneous Organic Catalytic Activities. *J. Phys. Chem. C* **2011**, *115* (31), 15288−15296.

(12) Liang, X.; Gao, L.; Yang, S.; Sun, J. Facile Synthesis and Shape Evolution of Single-Crystal Cuprous Oxide. *Adv. Mater.* **2009**, *21* (20), 2068−2071.

(13) Chen, K.; Xue, D. pH-Assisted Crystallization of Cu2O: Chemical Reactions Control the Evolution from Nanowires to Polyhedra. *CrystEngComm* **2012**, *14*, 8068−8075.

(14) Zhang, Y.; Deng, B.; Zhang, T.; Gao, D; Xu, A.-W. Shape Effects of Cu2O Polyhedral Microcrystals on Photocatalytic Activity. *J. Phys. Chem. C* **2010**, *114*, 5073−5079.

(15) Tan, C.; Hsu, S.; Ke, W.; Chen, L.; Huang, M. H. Facet-Dependent Electrical Conductivity Properties of Cu2O Crystals. *Nano Lett.* **2015**, *15* (15), 2155−2160.

(16) Kwon, Y.; Soon, A.; Han, H.; Lee, H. Shape Effects of Cuprous Oxide Particles on Stability in Water and Photocatalytic Water Splitting. *J. Mater. Chem. A* **2015**, *3* (1), 156−162.

(17) Xu, H.; Wang, W.; Zhu, W. Shape Evolution and Size-Controllable Synthesis of Cu2O Octahedra and Their Morphology-Dependent Photocatalytic Properties. *J. Phys. Chem. B* **2006**, *110*, 13829−13834.

(18) Chanda, K.; Rej, S.; Huang, M. H. Investigation of Facet Effects on the Catalytic Activity of Cu2O Nanocrystals for Efficient Regioselective Synthesis of 3,5-Disubstituted Isoxazoles. *Nanoscale* **2013**, *5* (24), 12494.

(19) Li, A.; Li, P.; Hu, J.; Zhang, W. Crystal-Facet-Controllable Synthesis of Cu2O Microcrystals, Shape Evolution and Their Comparative Photocatalytic Activity. *J. Mater. Sci.: Mater. Electron.* **2015**, *26*, 5071−5077.

(20) Ho, J. Y.; Huang, M. H. Synthesis of Submicrometer-Sized Cu2O Crystals with Morphological Evolution from Cubic to Hexapod Structures and Their Comparative Photocatalytic Activity. *J. Phys. Chem. C* **2009**, *113* (32), 14159−14164.

(21) Soon, A.; Todorova, M.; Delley, B.; Stampfl, C. Thermodynamic Stability and Structure of Copper Oxide Surfaces: A First-Principles Investigation. *Phys. Rev. B: Condens. Matter Mater. Phys.* **2007**, *75* (12), 1−9.

(22) Le, D.; Stolbov, S.; Rahman, T. S. Reactivity of the Cu2O (100) Surface: Insights from First Principles Calculations. *Surf. Sci.* **2009**, *603* (10−12), 1637−1645.
(23) Bendavid, L. I.; Carter, E. a. First-Principles Predictions of the Structure, Stability, and Photocatalytic Potential of Cu2O Surfaces. *J. Phys. Chem. B* **2013**, *117*, 15750−15760.
(24) Heyd, J.; Scuseria, G. E.; Ernzerhof, M. Hybrid Functionals Based on a Screened Coulomb Potential. *J. Chem. Phys.* **2003**, *118* (18), 8207−8215.
(25) Bylander, D. M.; Kleinman, L. Good Semiconductor Band Gaps with a Modified Local-Density Approximation. *Phys. Rev. B: Condens. Matter Mater. Phys.* **1990**, *41* (11), 7868−7871.
(26) Su, Y.; Nathan, A.; Ma, H.; Wang, H. Precise Control of Cu2O Nanostructures and LED-Assisted Photocatalysis. *RSC Adv.* **2016**, *6* (81), 78181−78186.
(27) Clark, S. J.; Segall, M. D.; Pickard, C. J.; Hasnip, P. J.; Probert, M. I. J.; Refson, K.; Payne, M. C. First Principles Methods Using CASTEP. *Z. Kristallogr. - Cryst. Mater.* **2005**, *220* (5/6), 567−570.
(28) Wang, M.; Sun, L.; Lin, Z.; Cai, J.; Xie, K.; Lin, C. P−n Heterojunction Photoelectrodes Composed of Cu2O-Loaded TiO2 Nanotube Arrays with Enhanced Photoelectrochemical and Photoelectrocatalytic Activities. *Energy Environ. Sci.* **2013**, *6* (4), 1211−1220.
(29) Chase, M. W. *NIST-JANAF Thermochemical Tables*; American Chemical Society,: New York, 1998.
(30) Ma, Y.; Li, X.; Yang, Z.; Xu, S.; Zhang, W.; Su, Y.; Hu, N.; Feng, J.; Zhang, Y. Morphology Control and Photocatalysis Enhancement by in-Situ Hybridization of Cu2O with Nitrogen-Doped Carbon Quantum Dots. *Langmuir* **2016**, *32*, 9418.

DOI: 10.1021/acsami.6b15648
ACS Appl. Mater. Interfaces 2017, 9, 8100−8106